DOI: 10.1002/ ((please add manuscript number))

Article type: Full Paper

Rational Design of Transparent Nanowire Architectures for Preventing Marine Fouling

Jing Wang, Sudarat Lee, Ashley R. Bielinski, Kevin A. Meyer, Abhishek Dhyani, Alondra M. Ortiz-Ortiz, Anish Tuteja, Neil P. Dasgupta**

Dr. Jing Wang, Dr. Sudarat Lee, Dr. Ashley R. Bielinski, Alondra M. Ortiz-Ortiz, Prof. Neil P. Dasgupta,

Department of Mechanical Engineering, University of Michigan, Ann Arbor, Michigan 48109, United States

Email: ndasgupt@umich.edu

Dr. Kevin A. Meyer,

School for Environment and Sustainability, University of Michigan, Ann Arbor, Michigan 48109, United States

Abhishek Dhyani, Prof. Anish Tuteja,

Department of Macromolecular Science and Engineering, University of Michigan, Ann Arbor, Michigan 48109, United States

Biointerfaces Institute, University of Michigan, Ann Arbor, Michigan 48109, United States

Prof. Anish Tuteja,

Department of Materials Science and Engineering, University of Michigan, Ann Arbor, Michigan 48109, United States

Department of Chemical Engineering, University of Michigan, Ann Arbor, Michigan 48109, United States

Email: atuteja@umich.edu

Keywords: Nanowires, Marine fouling, Superhydrophobic, Atomic layer deposition, Wetting

ABSTRACT

Marine biofouling is a sticky global problem that hinders maritime industries. Various micro-scale surface structures inspired by marine biological species have been explored for their anti-fouling properties. However, systematic studies of anti-marine-fouling performance on surface architectures with characteristic length-scales spanning from below 100 nm to greater than 10 μm are generally lacking. Herein, we present a study on the rational design and fabrication of ZnO/Al_2O_3 core-shell nanowire architectures with tunable geometries (length, spacing, branching) and surface chemistry. We demonstrate the ability of the nanowires to significantly delay or prevent marine biofouling. Compared to planar surfaces, hydrophilic nanowires can reduce fouling coverage by up to ~60% after 20 days. The fouling reduction mechanism is mainly due to two geometric effects: reduced effective settlement area and mechanical cell penetration. Additionally, superhydrophobic nanowires can completely prevent marine biofouling for up to 22 days. The nanowire surfaces are transparent across the visible spectrum, making them applicable to windows and oceanographic sensors. Through the rational control of surface nano-architectures, the coupled relationships between wettability, transparency, and anti-

biofouling performance are identified. We envision that the insights gained from the work can be used to systematically design surfaces that reduce marine biofouling in various industrial settings.

1. Introduction

Marine biofouling is a sticky global problem due to the vast diversity of fouling organisms and adhesion mechanisms that hinder a range of maritime applications [1]. Issues associated with marine biofouling include increased fuel consumption from drag [2], safety concerns from corrosion [3], and attenuation of sensor signals [4]. Challenges specific to the marine environment include development of robust fouling solutions for a diverse range of biological species and local ocean conditions, toxicity associated with commercial anti-fouling paints, and manufacturing challenges associated with coating a range of materials and non-planar geometries. For example, to prevent fouling on windows and other viewing surfaces, it is critical to maintain optical transparency. This prevents the potential use of common anti-fouling paints[5].

To overcome these challenges, surface micro/nano structures have attracted significant recent attention. This is in part because numerous marine species (e.g., shark skin [6], crab eyes [7], seashell [8]) have evolved to adopt surface micro/nano structures to prevent marine-fouling [9]. Inspired by these marine species, a range of structures with characteristic length-scales typically ranging from micrometers to millimeters have been designed and fabricated to reduce marine fouling [10]. Such surfaces have been tested within both single-species (e.g., *Ulva* spores, marine diatoms, barnacle larva) [10b, 10d] and multi-species (e.g., field tests in the ocean) [10a] environments. However, most of the surface microstructures studied to date have focused on reducing fouling of a single species; in

contrast, surface structuring has often demonstrated minimal reduction, or even an increase in fouling when exposed to a multi-species environment [10a, 10b].

Additionally, nano-scale surface structures (ranging from <100 nm to hundreds of nanometers) have been explored for their antibacterial properties in biomedical applications [11]. However, nano-scale surface architectures with tunable geometric control have not yet been systematical studied in marine fouling environments. It has been widely reported that marine biofouling follows a linear 'successional' model [1, 12] in which smaller species (cyanobacteria, etc.) settle and grow first, followed by spores of macroalgae (diatoms, etc.) within the first week, and finally within several weeks, by larvae of invertebrates (barnacles, etc.). Accordingly, we hypothesize that nanoscale structures can be used to impact the initial settlement and growth of marine cyanobacteria, and further prevent or delay subseuquent fouling based on the 'successional' model [1, 12]. In general, systematic studies of marine biofouling on surface architectures with characteristic length-scales that span a range from below 100 nm to above 10 µm could lead to new mechanistic insight into the development of anti-marine-fouling coatings, but are lacking.

One of the major challenges associated with systematically studying marine fouling on surface textures at these extremely small length-scales is the availability of scalable nano-fabrication processes that enable systematic tuning of feature geometries on a variety of non-planar substrates. Most current fabrication methods to create controlled nanoscale architectures depend on different patterning processes (e.g., lithography), which are restricted in their substrate compatibility, scalability, and cost [11a, 13]. In addition, it is challenging to apply lithography techniques to fabricate nanostructures on complex geometries, such as curved surfaces and fabrics. Alternative patterning and deposition methods (e.g., self-assembly) can provide precise control over periodic

geometries.[14] However, the ability to decouple independent geometric parameters in 3-dimensions (width, spacing, aspect ratio), which maintain conformal coverage over large areas and on non-planar surfaces is a challenge for many of these techniques.

Herein, we present a study on the rational design and systematic control of nanowire architectures with tunable geometric parameters (length, spacing, and branching), using atomic layer deposition (ALD) for surface-directed nucleation and growth of hydrothermal nanowires (NWs) [15]. We have previously demonstrated that this approach allows for the systematic fabrication of NW architectures independent of the underlying surface geometry or composition, and can be used to tune surface wetting to enable superomniphobic surfaces by design [15a].

In this study, the effect of surface chemistry and geometry on marine algal fouling in a multi-species environment are systematically studied for core-shell, or core-shell-shell, NW structures. It is shown that unfunctionalized NW structures can delay algal biofouling for ~15 days, and reduce the surface coverage of fouling by up to ~60% after 20 days compared to the untreated surfaces, while maintaining optical transparency. The mechanism of fouling reduction on the hydrophilic NWs can be attributed to two effects: 1) the NWs reduce the effective contact area with the fouling marine algae due to a steric hinderance to cell settlement; and 2) NWs produce a mechanical biocidal effect on the settled algae. The impact of NW geometry (length, spacing, and branching) on these effects was studied by systematic tuning the surface architecture.

Additionally, superhydrophobic NWs surfaces, fabricated by functionalizing the produced NWs with a low-surface-energy silane, demonstrated complete fouling prevention for ~20 days and reduced the fouling coverage for more than 50 days. The durability of the superhydrophobicity obtained on

different NW architectures can be explained through thermodynamic and mass transfer analysis and helps provide design principles for fabricating superhydrophobic anti-fouling coatings. In addition, the nanowire architectures were all transparent across the visible spectrum, demonstrating their feasibility on windows and optical surfaces. Overall, our work systematically discusses and demonstrates the design of anti-biofouling NW architectures with length-scales spanning from below 100 nm to greater than 10 µm. By decoupling the impacts of NW geometry and surface chemistry, this study provides new insights into the rational design of anti-marine-fouling coatings at the nanoscale.

2. Results and Discussion

2.1. Fabrication of NW surfaces

Marine algae are a complex mixture of diverse species with a characteristic size range from sub-micron to tens of micrometers (Figure S1). Therefore, to study the impacts on marine fouling of surface textures that span these length-scales, ZnO NW arrays with tunable length, spacing, and branching were prepared using a previously-published method of surface-directed assembly that combines ALD with hydrothermal NW growth [15] (see details in Experimental Section). Specifically, shown in Figures 1a and S2, the substrate (e.g., glass) was coated with a 20 nm seed layer of ALD ZnO, followed by a sub-monolayer "overlayer" of ALD TiO_2. By controlling the number of ALD TiO_2 cycles in this overlayer, the nucleation density of ZnO NWs can be monotonically tuned during subsequent hydrothermal growth with controlled inter-NW spacing from ~40 nm to >10 µm [15a]. As shown by scanning electron microscope (SEM) analysis, the length of the NWs was tuned by varying the hydrothermal growth time (Figure 1b), while the spacing of the NWs was tuned by increasing

with the number of ALD TiO_2 overlayer cycles (Figure 1c). In addition to controlling NW length and spacing, branched NWs (BNWs) with controlled spacing were fabricated by a multi-step ALD-seeding/hydrothermal growth process (Figure 1d and S2b) [15a]. Figure 1 shows a series of SEM images of the resulting NW and BNW morphologies to demonstrate the tunable control of the NW architecture. After the hydrothermal growth, the NWs were subsequently coated with a 5 nm Al_2O_3 shell to form a core-shell structure (Figure S2c). This shell served to prevent ZnO dissolution in the aqueous environment and enabled subsequent surface functionalization (further details in Experimental Section). Furthermore, the NWs can withstand normal shear flow (Figures S3 and S4, and Table S1) and strong fluid and acoustic cleaning process (Figure S5) (Supporting Information). Moreover, we demonstrated that this fabrication method can be applied to larger length scales and to non-planar surfaces (Figure S6 and Supporting Video S1).

2.2. Optical transparency characterization

The optical transparency of the NW architectures was characterized using UV-Vis spectrophotometry. As shown in Figure 2, all of the NW geometries were transparent across the visible spectrum, with an absorption onset in the ultraviolet region that corresponds to the bandgap of ZnO. For all high-density NWs (inter-NW spacing S <100nm) the samples transmitted >90% of light at wavelengths above 500 nm, and >80% between 400 nm and 500 nm (Figure 2a and 2b). The transmittance decreased with increasing inter-NW spacing, which can be attributed to diffused light scattering that results from a slight decrease in NW angle with respect to the substrate normal (Figure 1c). Following this trend, the branched NWs (BNWs) have a transmittance greater than 60%, which is attributed to increased scattering from the branches. In addition to total transmittance, the

haze for each sample was quantified to illustrate the optical clarity of the samples (Figure S7 and Supporting Information).

2.3. Wettability characterization

In order to decouple the roles of surface geometry and surface functionalization on marine fouling, we fabricated both hydrophilic and superhydrophobic NWs (Figure 3a) with tunable geometries. The ALD Al_2O_3 shell on the NWs is intrinsically hydrophilic due to its high surface energy (~900 mJ/m^2) [16], as confirmed by contact angle measurements (Figure 3b). Therefore, the wetted NWs in these hydrophilic samples were in the Wenzel state [17], which fully exposed the NW surfaces to the marine environment.

In contrast, superhydrophobic NWs were fabricated by surface functionalization of the NWs with a perfluorinated silane (see in Method). The water repellency of the silanized NWs was confirmed through contact angle and contact angle hysteresis measurements (Figure 3). The silanized NWs possessing small inter-NW spacing (<100 nm) and varying lengths were all superhydrophobic (Figure 3b). The contact angle increased slightly with increasing NW length, which can be explained by a slight increase in inter-NW spacing at the tips with increasing length (Figure 1b). As the silanized NW spacing was increased to be above ~3.2 μm, water wet the surface and entered the Wenzel state. This is because of the decrease in the breakthrough pressure, i.e. the applied pressure which forces the transition from the Cassie-Baxter State to the Wenzel State (see Figure 3a), with increasing NW spacing [18]. Furthermore, based on the modified Furmidge equation [19], we can estimate the sliding angles from the advancing and receding angles of each surface (Table S2 and S3). All of the BNWs were superhydrophobic with low contact angle hysteresis (Table S4). In addition, we demonstrated

that the superhydrophobic NWs are stable under hydrostatic pressure with DI water (depth: 300 mm for 10 days) (Figure S8), long exposure to seawater (1 month, Figure S9) and ambient environment (>1 year, Table S5).

2.4. Algal fouling on hydrophilic NWs

2.4.1. Algal fouling performance

We first studied the fouling of hydrophilic NWs (without silanization) as a function of geometry by submersing the samples in artificial seawater with 1-gram wet biomass of algae. The marine algae in this study were originally collected from the coast of Florida (USA), and have been previously utilized to study marine biofouling [2, 20]. The culture contains multiple species [2, 21] including cyanobacteria and diatoms (Figure S1). The sample area covered by fouling was imaged every day for 50 days using optical microscopy, and quantified using ImageJ analysis (see Experimental Section, Figure S10). As seen in the optical microscopy images (Figure 4a and Supporting Information) of the surfaces after 20 days fouling, all of the NW surfaces showed significant fouling reduction compared to the planar control.

Specifically, the planar control with the same surface chemistry as the NWs (5 nm ALD-coated Al_2O_3) was completely covered by fouling after ~20 days, while the hydrophilic NWs with different lengths and degrees of branching showed ~50% less coverage within the same time period (Figure 4b and 4c). Approximately 35 days were required for the hydrophilic NWs to be 100% covered with a biofilm, representing a delay of ~15 days compared to the control. From the data shown in Figure 4b and 4c, it is clear that the fouling rate on the hydrophilic samples was relatively independent of NW length and branching. In contrast, the fouling rate increased with increasing inter-NW spacing. From

Figure 4d, the areal coverage was ~50%, ~65%, ~75%, and ~90% after 20 days on NWs with a spacing of 0.05±0.01 μm, 0.43±0.17 μm, 1.40±0.49 μm, and 11.27±2.02 μm, respectively. To confirm that these trends were not a function of the algal concentration, we evaluated and observed the same relative fouling rates in an environment where the initial algae concentration was reduced by 50% (Figure S11).

The fouling coverage area fraction is a 2-dimensional projection of a 3-dimensional biofilm structure. To confirm that this is an accurate representation of the total extent of marine biofouling, we performed optical density measurements [22] on the fabricated surfaces after 20-days of fouling. In these tests, a staining dye is absorbed by the cells, which is subsequently dissolved into dimethyl sulfoxide (DMSO). By measuring the optical absorbance of the dye solution, a quantitative measurement of the total volume of cells attached to the surface can be obtained. As shown in Figure S12, the trends observed in the optical density measurements were in agreement with the areal coverage from optical microscopy, which indicates the uniformity of the biofilm across the fouled area on the surface, and further validates the use of the algae coverage area fraction as an quantitative measure of fouling extent.

2.4.2. Fouling reduction mechanism on hydrophilic NWs

The fouling reduction on the hydrophilic NWs can be attributed to two main factors: 1. Size-selective settlement of different marine species based on the inter-NW spacing; 2. A mechanical biocidal effect arising from deformation of the settled bacteria on the NW surfaces [11a, 11b, 23]. Each of these mechanisms are discussed in further detail below.

Size-Selective Settlement Mechanism: The first mechanism for the reduced fouling rate arises from our ability to tune the NW geometry at the characteristic length scales that match the size of the various fouling marine species (e.g. bacterial, diatoms). We observed the initial settlement of the marine algae on surfaces with different inter-NW spacings after 2-days of fouling. Cross-sectional SEM images (Figure 5a) demonstrate that the density of algae settlement between the NWs increased with increasing inter-NW spacing (further details in the Supporting Information). Specifically, when the inter-NW spacing was larger than ~300 nm, bacteria were observed in the gaps between NWs. In contrast, for smaller inter-NW spacings, no settlement was observed between the NWs, and bacteria were only able to settle on the top surface of the NW array. We attribute this to steric hinderance, as the smallest length-scale of bacteria observed was ~200 nm. Similarly, diatom settlement between the NWs was only observed when the inter-NW spacing was greater than 10 μm, which is the characteristic size of the diatoms observed in this study. Further statistical analysis of these trends at different locations along the surface are provided in the Supporting Information (Figure S13). These trends illustrate that the fouling species are able to access a larger fraction of the surface area for settlement as the inter-NW spacing increases (Figure 5b).

To reconcile these initial settlement observations with the fouling coverage area fraction results after extended time (shown in Figure 4d), we propose the following mechanism. When the inter-NW spacing is smaller than the characteristic length scale of bacteria, the rate of settlement between the NWs is very small, and therefore, the settlement focuses at the top surfaces of the NWs. This represents a smaller effective surface area than a planar sample, since the contact points are only at the tips of the NW. As discussed in the second mechanism below, this tip-contact with the cells also leads to a mechanical bactericidal effect.

As the inter-NW spacing increases within the range of 300 nm-10 μm, the accessible surface for settlement increases, and bacteria are able to grow within the inter-NW voids. This mechanism increases the fouling rate as the inter-NW spacing increases. Eventually, as the inter-NW spacing continues to increase, a larger fraction of the underlying planar surface is available for settlement. The planar surface facilitates settlement of a more diverse range of species, including diatoms. These trends indicate that the modulation of initial settlement can have a strong impact on the longer-term bio-fouling growth rate, as shown in Figure 5c.

Mechanical Biocidal Effect: The second mechanism for reducing the fouling rate on the NW surfaces relates to the biocidal effect that arises from mechanical interactions between the NWs and bacteria. This effect is known within the natural world; for example, dragonfly/cicada wings have strong bactericidal properties that arise from their nanostructured surfaces [11a, 11d]. These effects have been shown to be independent of surface chemical composition, and arise from the surface texture, rather than material toxicity.

To demonstrate that our NW arrays possess similar biocidal properties, we analyzed the surfaces after 5 days of fouling test through fluorescent microscopic imaging using live/dead bacteria stains [24]. In Figure 6a, we observe an increased fluorescence signal from total-cell dye (fluorescent color: green) as inter-NW spacing increases. This is consistent with the trends shown in Figure 4d, wherein the fouling rate increases with increasing inter-NW spacing. Furthermore, we observed that the fraction of total cells that are dead (fluorescent color: red) decreases as inter-NW spacing increases. Similar trends are observed in the hydrophilic NW samples with different NW lengths and degrees of branching (Figures S14 and S15). This indicates that as the inter-NW spacing decreases, a mechanical biocidal effect, similar to naturally nanostructured anti-bacterial surfaces, can be observed. This

leads to the death of the initial bacteria that settle on the closely-packed NW surfaces, and slows the subsequent bio-film growth kinetics.

To confirm that this biocidal effect is purely a geometric effect and not caused by Zn-ion dissolution into the aqueous solution, we performed inductively coupled plasma mass spectrometry (ICP-MS) measurements (Figure S17). Owing to the presence of the Al_2O_3 shell on the NW surfaces, the concentration of Zn ions in the solution was found to be well below the toxicity level for marine algae [25]. Therefore, we conclude that it is the physical geometry, rather than the chemical composition of the NWs, that leads to their anti-bacterial properties.

These results on the mechanical toxicity of the fabricated NWs towards marine algae are consistent with previous studies on the anti-bacterial properties of other nanoscale surface architectures (e.g., black silicon [11a] and graphite [26]). Mechanical biocidal effects have been attributed to multiple mechanisms, for example, mechanical penetration of the cells [11a], destructive extraction [27], and storage and release of mechanical energy [11b]. While a full mechanistic understanding of these coupled mechanical-biocidal effect requires further investigation, it is clear that the rational design of hydrophilic NW architectures can be used to tune size-selective settlement and mechanical interactions during the initial settlement, which can both contribute to improved anti-fouling performance.

2.5. Algal fouling on superhydrophobic NWs

2.5.1. Algal fouling performance

To study the effect of surface wettability on marine fouling, superhydrophobic NWs were functionalized via reaction with a low-surface-energy fluoro-silane, and tested under the same

marine environment (Figure 7a and Supporting Information). For high-density superhydrophobic NWs with varying lengths, fouling was completely prevented for 7-12 days, and the time to reach 100% area coverage was 28-35 days longer than the planar control with the same surface chemistry (i.e., functionalized with fluoro-silane) (see Figure 7b). An increase in the length of the NWs resulted in a monotonic increase in the duration of the Cassie-Baxter state underwater, as shown by the increased residence time before the onset of fouling.

Furthermore, unlike the branched NWs (BNWs) in Wenzel state (Figure 6c), the BNWs in the Cassie-Baxter state exhibited an increased duration in fouling prevention compared to unbranched NWs (Figure 7c). Specifically, the BNWs remained un-fouled for 17 – 22 days, a period of greater than 50 days transpired before full algal areal coverage was observed on these surfaces (see in Figure 7c).

The fouling performance of the hydrophobic NWs was also observed to vary with the inter-NW spacing. Since NWs with a spacing of 11.27±2.02 μm were in Wenzel state even after silanization (Figure 3b), their fouling performance was similar to the unsilanized (hydrophilic) surfaces with large inter-NW spacing. This indicates changing surface chemistry alone does not have a strong effect on the NW's anti-fouling properties when wetting occurs. Similarly, the algal fouling coverage was close to the planar control (Figures 4d and 7d) when the inter-NW spacing was greater than 10 μm.

In contrast, when the inter-NW spacing was small enough to maintain the Cassie-Baxter state, a minimum in surface fouling as a function of NW spacing was observed. Specifically, the NWs with an intermediate spacing of S = 0.43±0.17 μm outperformed the NWs with smaller (S = 0.04±0.01 μm) and larger (S = 1.40±0.49 μm) spacing. The NWs with a spacing of 0.43 μm were completely un-fouled for more than 20 days, and increased the time required to reach 100% areal fouling coverage

by >50 days when compared to the planar control (Figure 7d). As with the hydrophilic samples, we performed optical density measurements a on the hydrophobic surfaces, and the results were found to be consistent with the trends observed in the 2-D areal coverage data (Figure S12).

2.5.2. Anti-fouling mechanism and superhydrophobicity duration on submerged NWs

To confirm that fouling was completely suppressed on superhydrophobic NWs before wetting occurs, the absence of any settled marine species on the solid surfaces was confirmed by fluorescent microscopy. All surface geometries were immersed in the marine algae culture solution for 5 days and then dyed with live/dead cell fluorescent dyes. As shown in Figure S14 and S16, NWs in the Cassie-Baxter state showed no fluorescent signal, as there were no cells attached to the surface. However, the samples that were initially superhydrophobic eventually became wetted by the marine environment and collapsed into the Wenzel state. At this point, fouling initiated.

Since the transition from the Cassie-Baxter state to the Wenzel state drove the onset of fouling, the underwater duration of superhydrophobicity (i.e., the time for which the air layer remained "trapped" within the NW texture) is critical in determining the longevity of fouling prevention. In general, the underwater duration of superhydrophobicity depends on the total volume of the air layer, the applied hydrostatic pressure, and follows Fick's law of mass transfer at the air-water interface [28]. Specifically, the underwater duration of the air layer within the NW texture can be expressed as:

$$\tau \sim V \cdot p^n \quad (1)$$

where τ is the duration of the air layer, V is the total volume of the air layer, p is hydrostatic pressure, and n is a constant depending on water properties (e.g., surface tension, oxygen and

nitrogen level, etc.) and any present contaminants (e.g., biological species, ionic concentration, organic contaminants, etc.) (further details in Supporting Information).

Furthermore, water is known to vaporize at a different rate along curved air-water interfaces due to an increase in the Laplace pressure. Quantitatively this change in vapor pressure is typically described by the Kelvin relation. This additional evaporation along a curved interface can be used to increase the stability of the gas layer when the surface pores are below a critical length (typically ~ 1 μm) [29]. Thus, to enhance the longevity of the superhydrophobic surfaces underwater, superhydrophobic NWs with a larger air volume and a spacing below 1 μm are desired.

From Figures 8a and S18, the superhydrophobic duration under the marine algae environment increased with the increase of the air layer volume on NWs with different length and degrees of hierarchy. Specifically, when the inter-NW spacing is fixed, the superhydrophobic duration on these surfaces increases linearly with the total volume of the air layer. In addition, the superhydrophobic duration increased with an increase in inter-NW spacing, when the spacing was less than the critical length (~1 μm) (Figure 8a) [29]. This is because the air layer volume increases with increasing inter-NW spacing, and all NWs with a spacing below 1 μm experience an enhancement in the superhydrophobicity duration as a result of the enhanced water vaporization. The vaporized water can partially replenish the air layer volume within submerged air-pockets, and thereby increase the lifetime.

In contrast, when the spacing of the NWs is larger than the critical length, the superhydrophobic duration decreases (Figure 8a). Interestingly, when the BNW architectures had a spacing between the base NWs of ~1.40 μm (larger than the critical length) the superhydrophobic duration still

increased. We attribute this to the fact that the spacing between the NW branches remained less than 1 μm, and thus the overall NW architecture possessed air pockets that can be stabilized by vaporized water. This demonstrates the utility provided by the control of hierarchical geometry at the nanoscale to tune the coupled wetting and fouling properties of superhydrophobic surfaces, and elucidates a set of design guidelines for nanostructured anti-fouling surfaces.

3. Conclusion

In this study, we fabricated optically-transparent nanostructured surfaces with controlled geometric parameters, and systematically studied their structure-property relationships with respect to marine fouling. As part of our work, we fabricated NW surfaces with tunable control over their length, inter-NW spacing, and degrees of hierarchy spanning the nano-to-micro scales.

For hydrophilic NWs, we demonstrated fouling reduction by up to 60% after 20 days, and a time-delay of 20 days before 100% fouling coverage. These anti-fouling properties were attributed to both size-selective settlement behavior and mechanical biocidal effects. For superhydrophobic NWs, we demonstrated that the non-fouling state can be maintained for up to 22 days and fouling can be delayed by more than 50 days.

By quantifying the coupled relationships between NW geometry, surface wettability, optical transparency, and interaction with marine algae, we have identified design guidelines that are supported by thermodynamic and mass transfer principles. Specifically, for hydrophilic NWs, the rate of fouling monotonically decreases with inter-NW spacing down to 50 nm, which is attributed to a combination of 1) size-selective settlement of marine species; and 2) a mechanical biocidal effect that arises from interactions at the NW tips. For superhydrophobic NWs, fouling can be completely

suppressed when the unwetted Cassie-Baxter state is maintained, and can be delayed when the NWs transit to the wetted Wenzel state due to the same reasons described for hydrophilic NWs. The duration of underwater superhydrophobicity can be enhanced by increasing the volume of the air layer (through increasing NW length and introducing hierarchical branching) and optimizing inter-NW spacing. In the future, the geometric design principles and mechanistic insights provided in this study could be applied to other nanostructured material systems, including durable polymer surfaces [30]. These insights can be used to rationally design nanostructured surfaces with anti-fouling properties for a broad range of applications, including marine fouling, biomedical devices, and the food industry.

4. Experimental Section

Atomic Layer Deposition: ZnO was deposited at a substrate temperature of 150 °C using diethyl zinc (DEZ) and DI water as the precursors. The ZnO deposited as a polycrystalline film with a growth rate of ~2.0 Å/cycle. TiO_2 was deposited at a substrate temperature of 175 °C using tetrakis(dimethylamido)titanium (TDMAT) and DI water as the precursors. The TiO_2 growth rate was measured to be ~0.6 Å/cycle using ellipsometry. Al_2O_3 was deposited at a substrate temperature of 150 °C using trimethylaluminum (TMA) and DI water as the precursors. The Al_2O_3 growth rate was measured to be ~1.0 Å/cycle using ellipsometry.

ZnO NW fabrication: The ZnO NWs were grown in a solution using the sample concentration from our previous report [15a]. The hydrothermal growth was performed at 90 °C and ambient pressure. The substrates with ALD seed layers were suspended facing downward with angle ~45^o in the

solution to prevent the homogeneous precipitate from settling on the surface. The total time for NW growth varied from 15 – 105 min after the solution temperature reached 90°C. To avoid overheating the solution, we gradually heated the solution from room temperature (20°C) to the reaction temperature (90 °C) at a rate of ~1°C/min. Therefore, the total submerged time for the samples varied between 75 – 165 minutes.

Surface chemistry modification: Heptadecafluoro-1,1,2,2-tetrahydrodecyltrichlorosilane (F-17) purchased from Gelest Inc. was used to silanize the core-shell ZnO/Al_2O_3 NWs with different lengths, inter-NW spacings, and levels of branching to achieve superhydrophobicity. 30 cycles ALD Al_2O_3 (~5 nm) was deposited on the NW surface as a buffer to provide reactive sites for silanization. The samples were cleaned in oxygen plasma for 10 min and maintained in a silane vapor environment at 120 °C for more than 3 hours. After silanization process, the samples were rinsed with toluene to remove unbonded silane. The perfluorinated silane used to render the NWs to be superhydrophobic was chosen as an example surface functionalization to explore the geometric design principles for underwater superhydrophobic surfaces. Other alternative biocompatible surface modifications can also be applied to make NWs superhydrophobic, for example, the grafting of polydimethylsiloxane (PDMS) chains [31].

Contact Angle Measurements: Contact angle measurements were performed with a Ramé-Hart 200-F1 contact angle goniometer using the sessile drop method. DI water and hexadecane, (purchased from Fisher Scientific) were used as probe liquids. Advancing and receding contact angles were obtained by measuring the angle while the liquid was slowly added to or removed from a ~3 µL droplet in contact with the sample and a micrometer syringe. At least five measurements were performed per sample, and the standard error is ±0.1°.

Algal Fouling Experiments: Marine green algae were raised in a fish tank at 25 ^{o}C with a standard bubbler and lighting for half-day on as a reservoir for algae biofilms. 40% of the total volume was replaced with fresh culture solution every week. 1 gram of biomass (i.e., algae biofilm) was weighted through an analytical balance with a resolution of 0.0001 gram and was introduced to a medium size petri dish (diameter: 100 mm) with 50 ml of seawater and F/2 (purchased from Amazon.com) mixture. Samples were cut into the same size (25 mm×15 mm) before fabrication and submerged into the algae culture environment after being coated with different NWs. The bench culture in petri dishes was kept in room temperature (20 ^{o}C) with a lighting for half-day on. 40% of the total volume (20 ml) was replace in each petri dish culture with fresh culture solution every 5 days. The hydrostatic pressure on the testing samples were kept at ~100 Pa.

Algae Coverage Area Fraction Measurement: The area fraction was quantified with microscopic images on the samples through ImageJ analysis. The microscopic images were taken over at least 3 different locations on each of the sample surfaces. The images were converted to 8-bit gray images and analyzed using ImageJ to obtain area coverage fraction. In supporting information, we show three microscopic images (Figure S10a) at different measurement spots on the hydrophilic NW sample after 20 days of fouling. In addition, in Figure S10b, we show the ImageJ analysis process on one of the microscopic images.

Optical Density Measurements: All samples were submerged in the algae culture solution for 20 days and rinsed by saltwater (0.8 M NaCl) to remove unattached algae. Then the samples were submerged in dimethyl sulfoxide (DMSO from Sigma Aldrich) for 15 min to remove the chlorophyll in the algae, which would interference the signal of the Trypan blue. After removing the chlorophyll, the samples were gently rinsed by saltwater again and stained with Trypan blue (from Thermal

Fisher) for 15 min, followed by rinsing off the excess dye. Finally, 10 ml of DMSO was used for each sample to extract the blue dye and absorbance of the liquid was measured by UV-VIS spectrometry.

Fluorescent Microscope Imaging: The samples were all submerged in the algal culture solution for 5 days, and then were taken out and placed in sodium chloride (NaCl) solution (0.85%) with gentle stirring for 15 min to remove the unsettled algae. We used a live/dead baclight bacteria dye kit (Thermofisher L7012) to stain the fouled samples. The mixing ratio of live/dead dye is 1:1, and the mixing ratio of dye to solution is 3 µl of dye to 1 ml of 0.85% NaCl. The samples were all stained with the dye solution for 15 min in dark environment. Fluorescent microscope images of each sample were taken through spinning disk confocal microscope (Olympus IX2-ZDC2) under the light with a wavelength of 480/500 nm (green) for total cells and 490/635 nm (red) for dead cells.

ICP-MS Measurements: A Zn ion calibration solution was prepared with concentrations of 5 ppb, 10 ppb, and 20 ppb. The measured concentration matched well with calibrated concentration and fitted linearly with R square >0.999. The NW samples, with protection Al_2O_3 ALD overcoats in ~5 nm and ~15 nm, were submerged into 2 ml of DI water for 5 days. The fouling testing environment for each sample was 50 ml.

Supporting Information

Supporting Information is available from the Wiley Online Library or from the author.

Acknowledgements

This work was supported by DARPA Young Faculty Award D18AP00066. Any opinions, findings, conclusions or recommendations expressed in this publication are those of the authors and do not necessarily reflect the views of DARPA. This material is based upon work supported by the National Science Foundation under grant no. 1751590. We thank Dr. James Gose at the Aaron Friedman Marine Hydrodynamics Laboratory of The University of Michigan for providing us the marine algae, Jacob Hoffman for assistance with the algae fouling experimenst, Maxwell DeNies and Prof. Allen Liu in Mechanical Engineering in University of Michigan for assistance with fluorescent microscopic imaging, and Tae Cho and Dr. Eric Kazyak for assistance with electron microscopy imaging.

Conflict of Interest

The authors have filed a provisional U.S. patent application related to this work.

Received: ((will be filled in by the editorial staff))
Revised: ((will be filled in by the editorial staff))
Published online: ((will be filled in by the editorial staff))

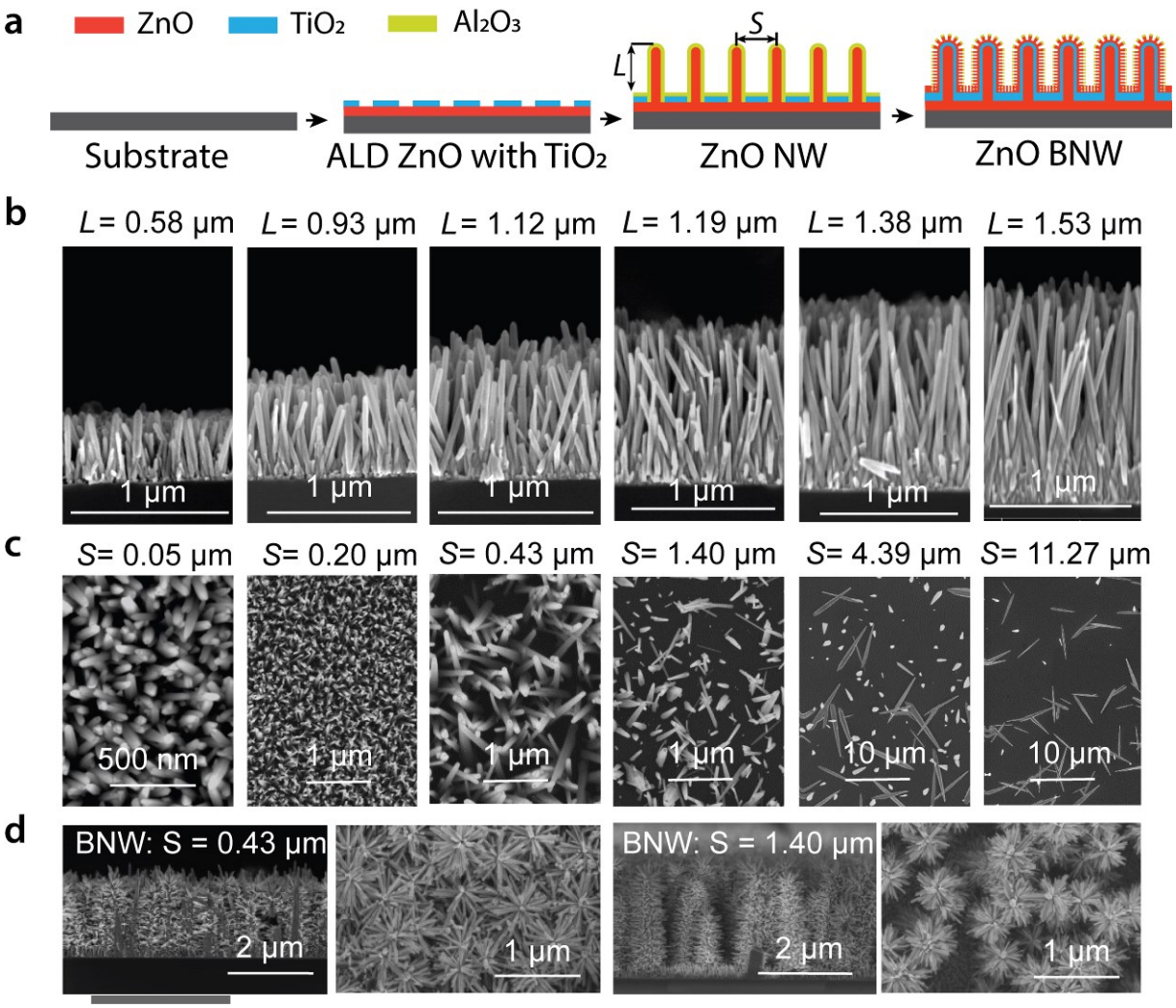

Figure 1. Fabrication of nanowires with tunable geometries. a, A schematic illustrating the NW fabrication process. b, SEM images of NWs with different lengths (*L*) ranging from 0.58 μm to 1.53 μm fabricated using different hydrothermal growth time from 15 min to 105 min. These NWs have similar inter-NW spacing as ~0.05 μm. c, SEM images of NWs with different inter-NW spacing (*S*) ranging from 0.05 μm to 11.37 μm. These NWs have similar NW length as ~1.50 μm. The inter-NW spacing was modulated by changing the number of ALD TiO_2 cycles from 0 cycle to 7 cycles. d, Branched NWs with varying spacing between the base NWs.

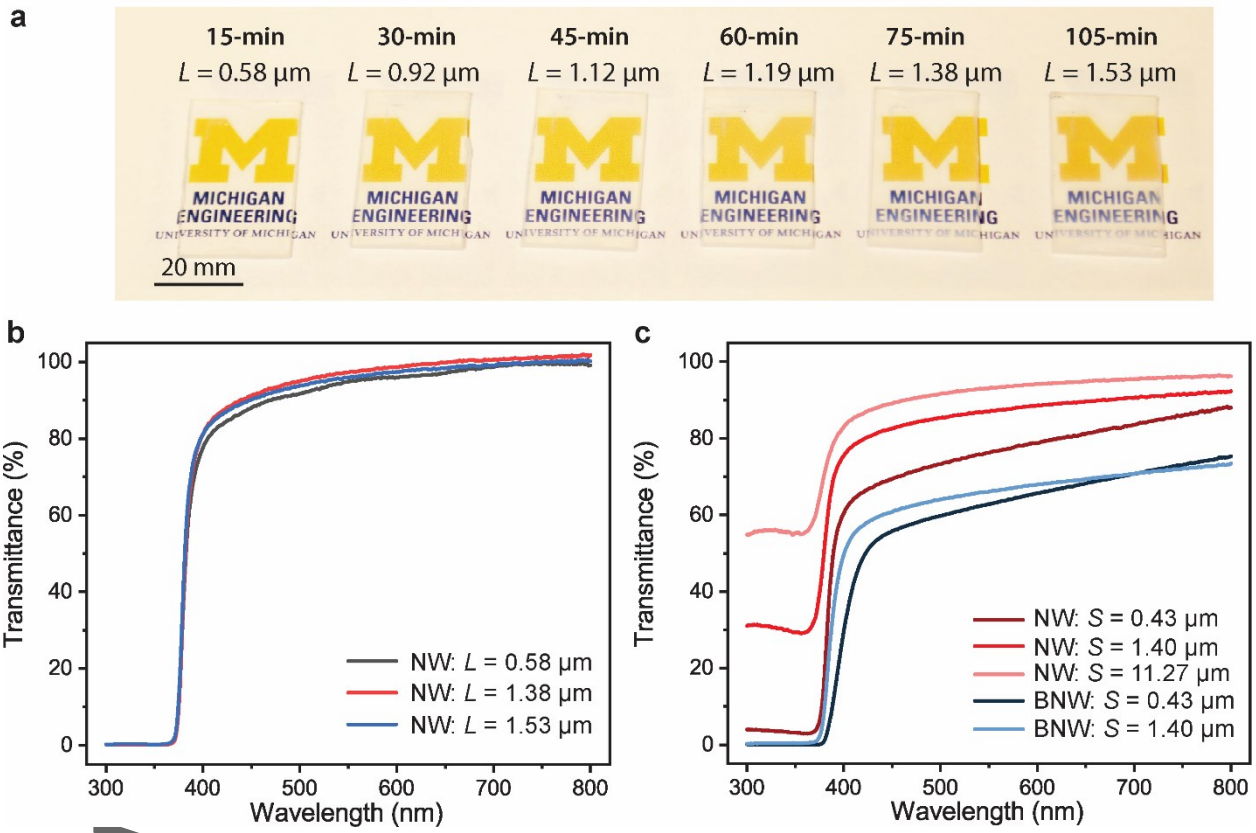

Figure 2. Optical characterization on the different nanowire surfaces fabricated on glass. a, Optical image demonstrating the transparency of the fabricated NW surfaces. b, Transmittance of NWs with different lengths and similar inter-NW spacing (~0.05 µm). c, Transmittance of NWs with different inter-NW spacing and branching and similar NW length (~1.50 µm).

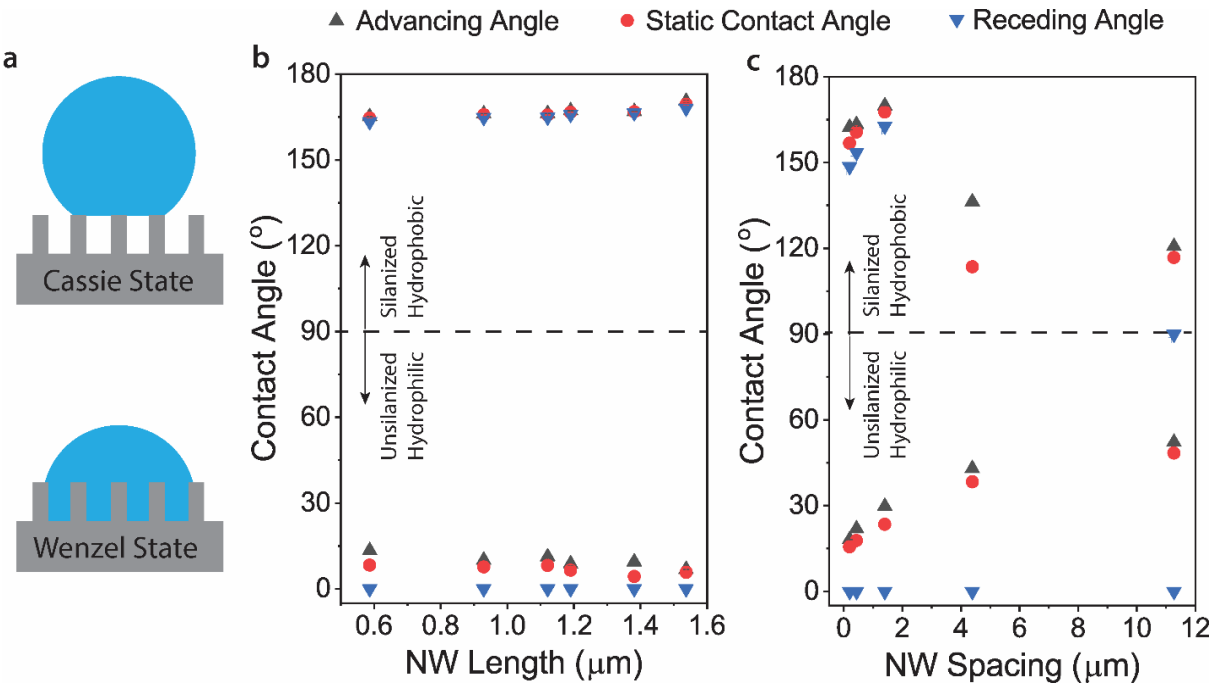

Figure 3. Contact angle measurement on hydrophobic NWs. a, Schematics illustrating Cassie-Baxter and Wenzel states. b, Contact angle and contact angle hysteresis measurements on unsilanized and silanized NWs with different lengths. c, Contact angle and contact angle hysteresis measurements on unsilanized and silanized NWs with different inter NW spacings. Error bars were obtained from at least 5 independent measurements.

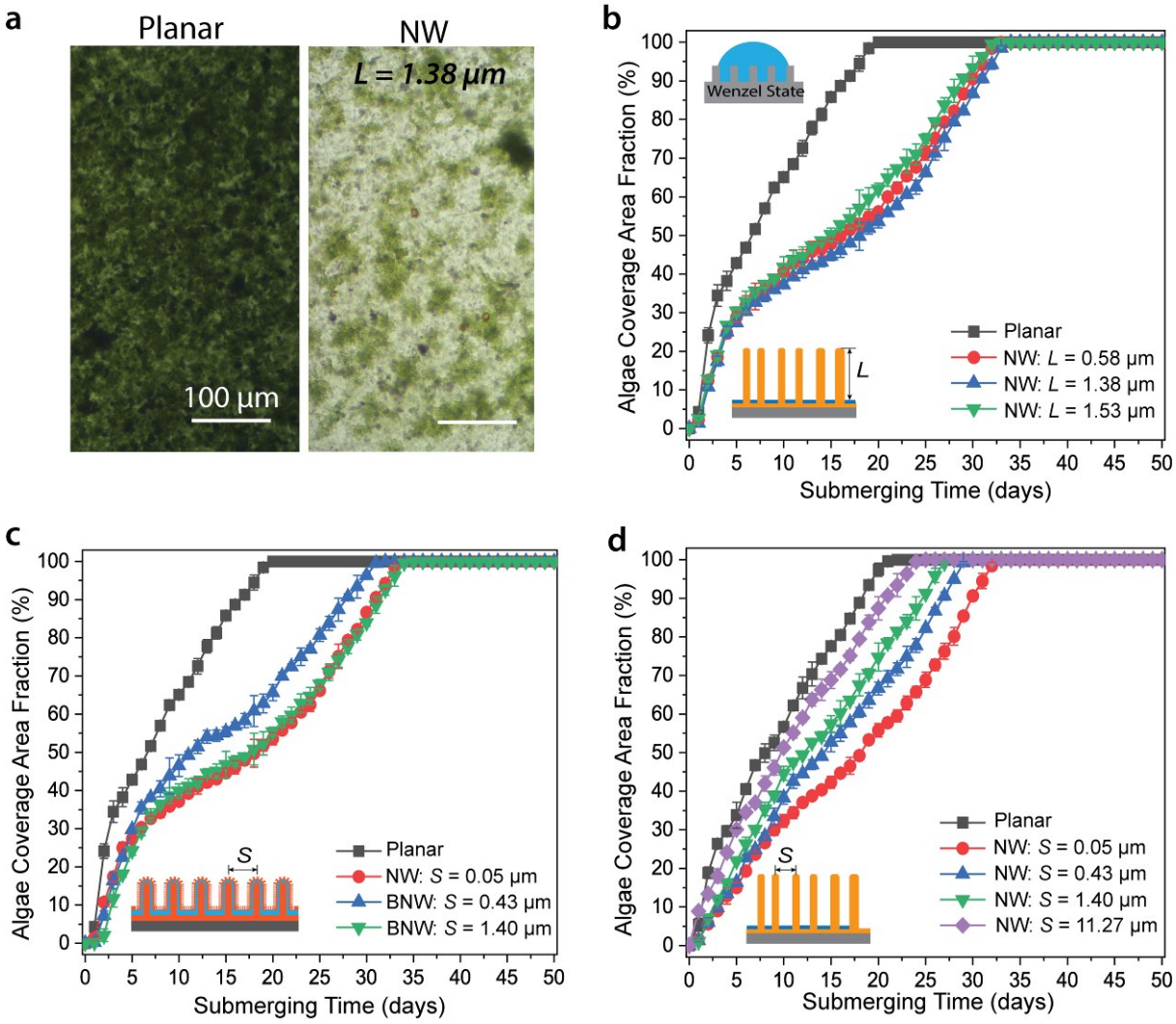

Figure 4. Marine algae fouling on different hydrophilic nanowire surfaces. a, Optical microscopy images comparing hydrophilic NW and planar control surfaces after 20 days of algal fouling. b, Algae coverage area fraction on NWs with different lengths and similar spacing (~0.05 μm) in the Wenzel state for 50 days. c, Algae coverage area fraction on BNWs in the Wenzel state for 50 days. d, Algae coverage area fraction on NWs with different inter-NW spacings and similar length (~1.50 μm) in the Wenzel state for 50 days. Errors bars were obtained from at least 3 independent measurements.

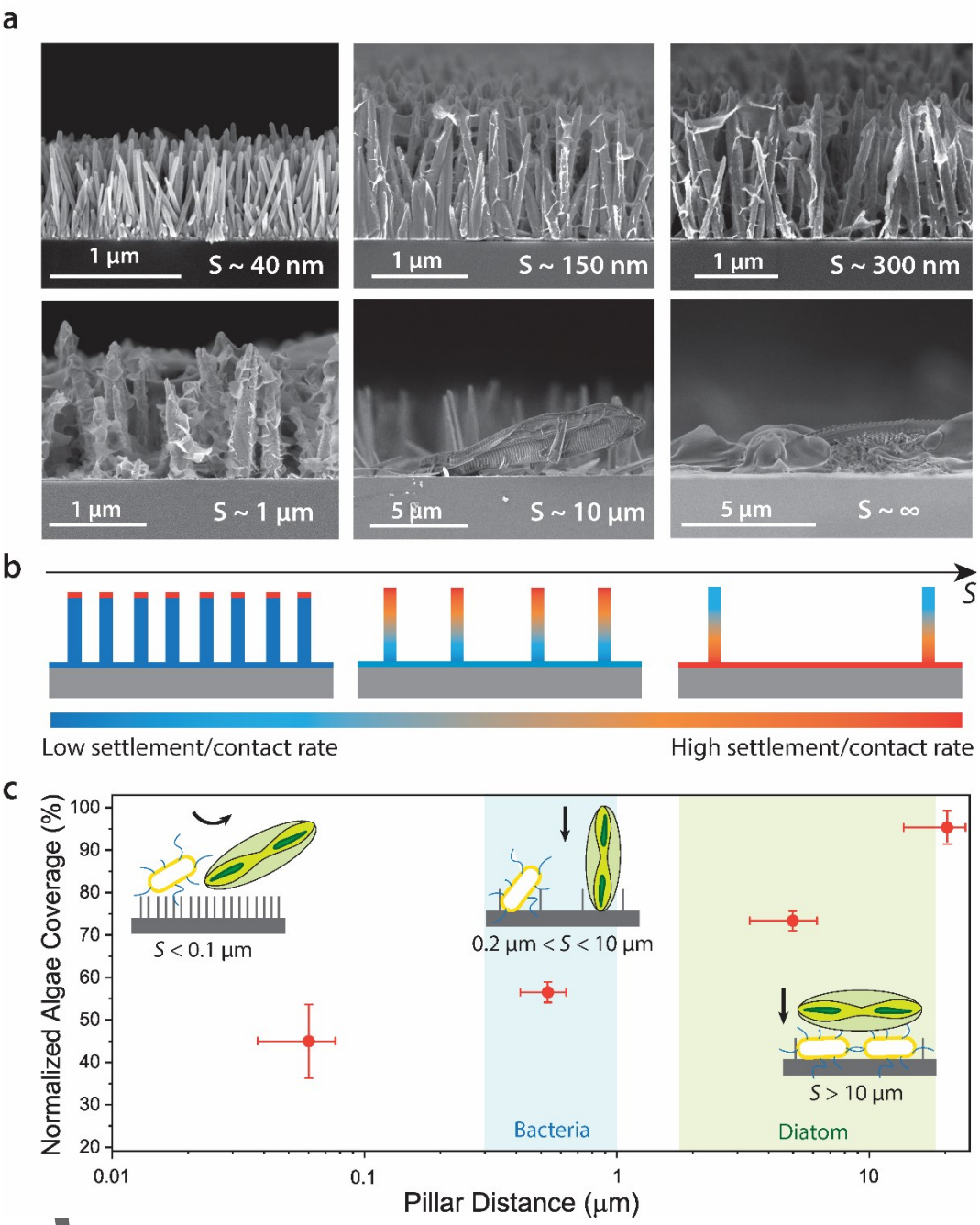

Figure 5. Size-selective settlement mechanism for fouling reduction on hydrophilic NWs. a, Cross-sectional SEM images of NWs with different spacing after 2-day fouling. b, Schematic illustrating the spatial variation in fouling rate along the surface of NWs with different spacings. c, The algal fouling

coverage area fraction, which has been normalized by the planar control on NWs with different spacings after 20 days. Errors bars were obtained from at least 3 independent measurements.

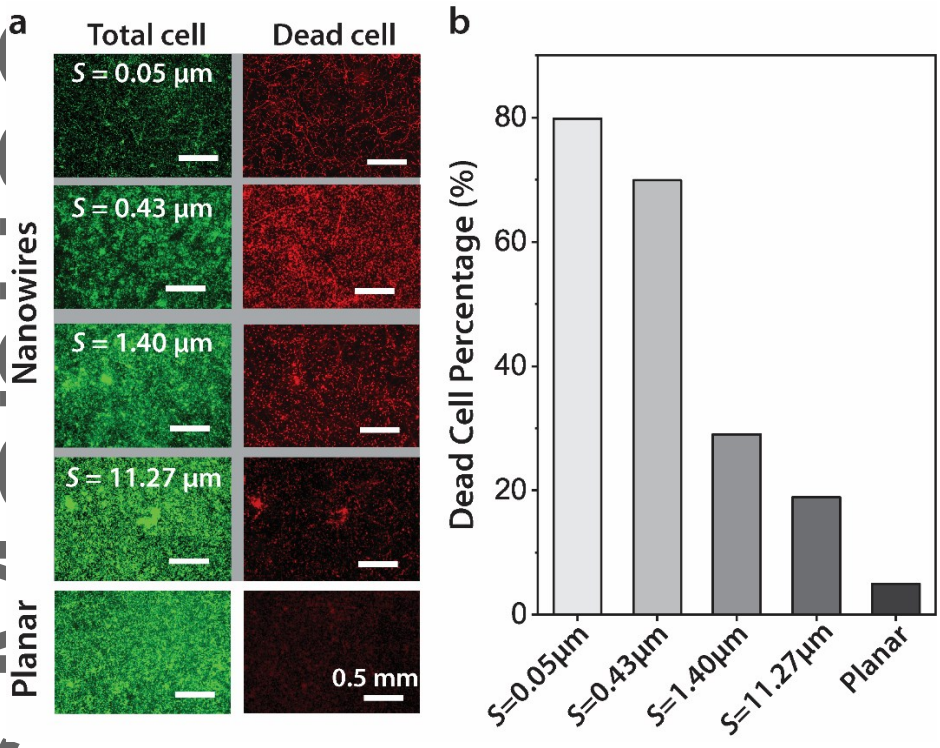

Figure 6. Mechanical biocidal effect of hydrophilic NWs. a, Fluorescent microscopic images of NWs with different inter-NW spacing after submerging in marine algae culture solution for 5 days. b, Dead cell percentage as a function of substrate geometry.

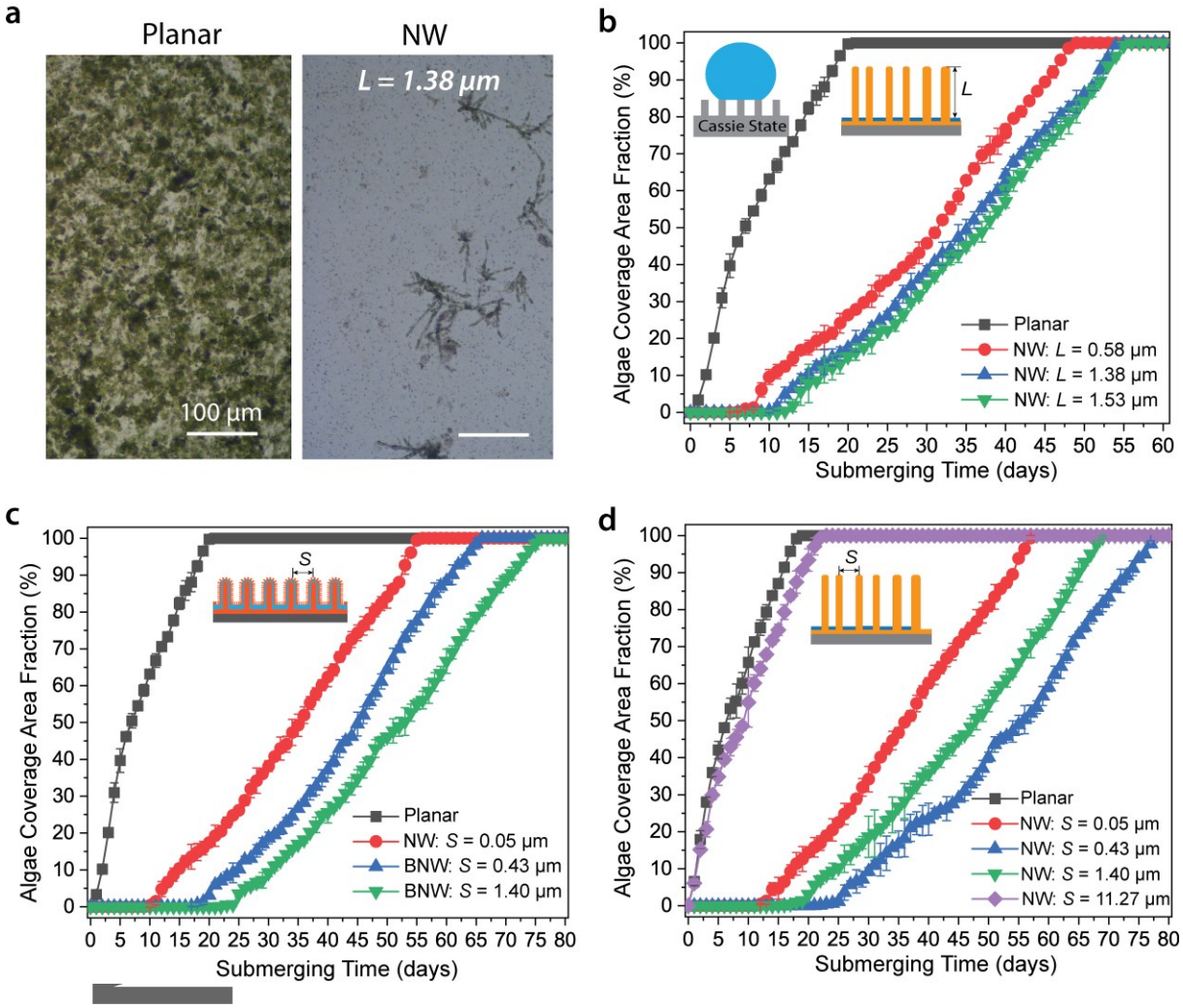

Figure 7. Marine algae fouling coverage on superhydrophobic nanowires surfaces. a, Optical microscopy images for planar and NW surfaces after 20 days of algae fouling. b, Algae coverage area fraction on high-density NWs as a function of NW length for 60 days. The inter-NW spacing of these NWs was ~0.05 μm c, Algae coverage area fraction on BNWs for 80 days. d, Algae coverage area on NWs with different inter-NW spacings and similar length (~1.50 μm) for 80 days. The immersion depth for all samples was 10 mm. Errors bars were obtained from at least 3 independent measurements.

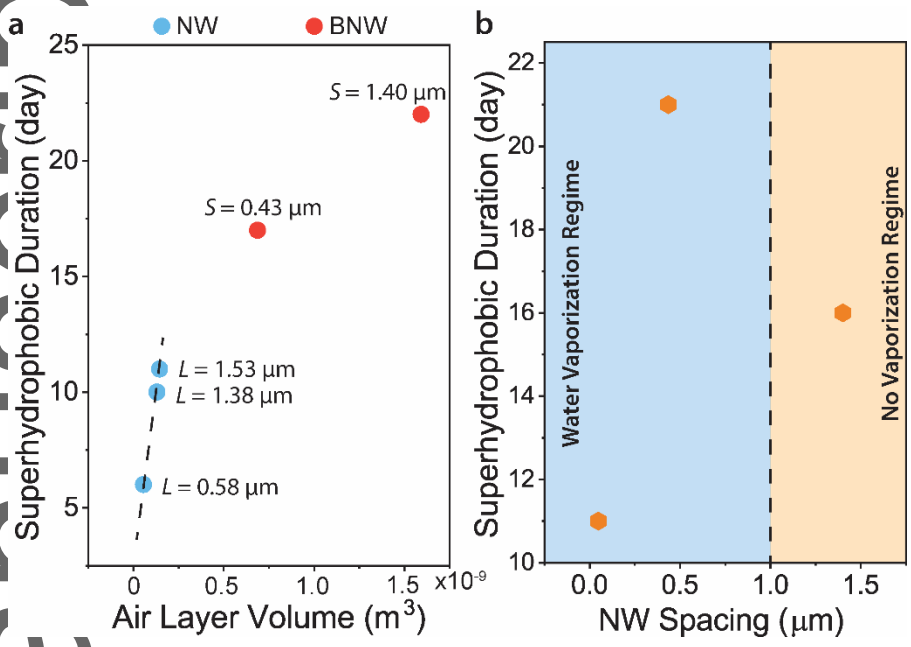

Figure 8. Superhydropobic duration for NWs in the Cassie-Baxter state. a, Superhydrophobicity duration of NW surfaces with different length and degrees of hierarchy under marine algae fouling conditions. b, Superhydrophobic duration of NW surfaces with different spacing under the marine algae fouling conditions.

Table of Contents Entry

Core-shell nanowire architectures with tunable geometries (length, spacing, branching) and surface chemistry are shown to significantly delay marine biofouling. The fouling reduction mechanism is mainly due to two effects: reduced effective settlement area and mechanical cell penetration. We

envision that the insights gained from the work can be used to systematically design surfaces that reduce marine biofouling in various industrial settings.

Keywords: Nanowires, Marine fouling, Superhydrophobic, Atomic layer deposition, Wetting

Jing Wang, Sudarat Lee, Ashley R. Bielinski, Kevin A. Meyer, Abhishek Dhyani, Alondra M. Ortiz-Ortiz, Anish Tuteja*, Neil P. Dasgupta*

Rational Design of Transparent Nanowire Architectures for Preventing Marine Fouling

ToC figure

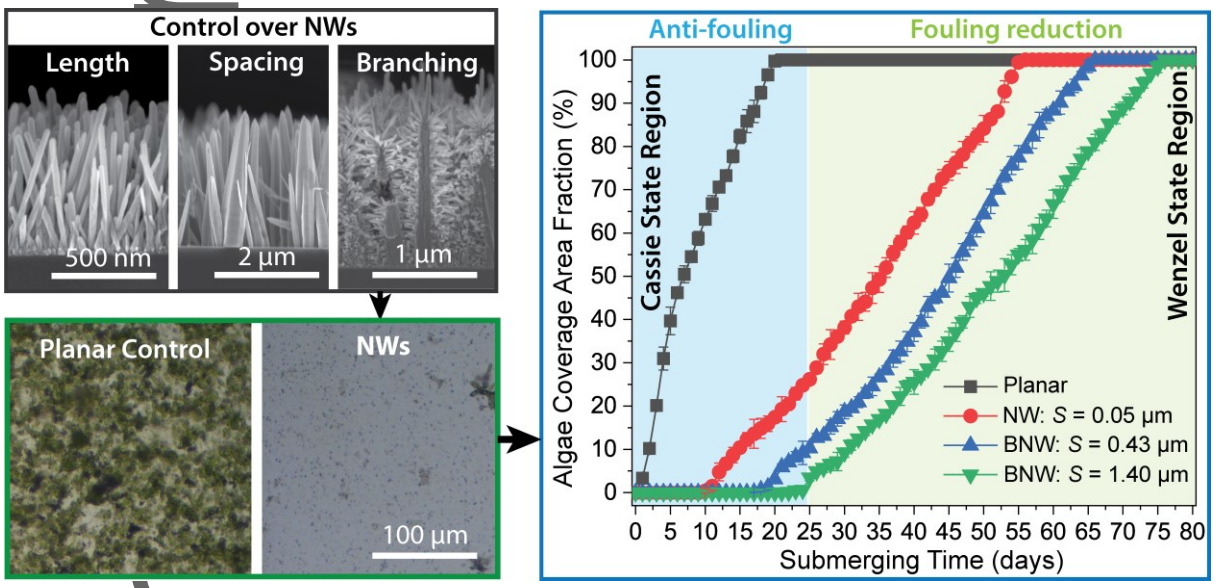

References

[1] J. A. Callow, M. E. Callow, *Nature Communications* **2011**, 2, 244.

[2] M. Schultz, J. Walker, C. Steppe, K. Flack, *Biofouling* **2015**, 31, 759.

[3] H. A. Videla, L. K. Herrera, *International microbiology* **2005**, 8, 169.

[4] L. Delauney, C. Compere, M. Lehaitre, *Ocean Science* **2010**, 6, 503.

[5] D. V. Manov, G. C. Chang, T. D. Dickey, *Journal of Atmospheric and Oceanic Technology* **2004**, 21, 958.

[6] J. F. Schumacher, C. J. Long, M. E. Callow, J. A. Finlay, J. A. Callow, A. B. Brennan, *Langmuir* **2008**, 24, 4931.

[7] G. Greco, T. S. Lanero, S. Torrassa, R. Young, M. Vassalli, A. Cavaliere, R. Rolandi, E. Pelucchi, M. Faimali, J. Davenport, *Journal of the Royal Society Interface* **2013**, 10, 20130122.

[8] A. Scardino, D. Hudleston, Z. Peng, N. A. Paul, R. De Nys, *Biofouling* **2009**, 25, 83.

[9] A. J. Scardino, R. de Nys, *Biofouling* **2011**, 27, 73.

[10] a) M. Vucko, A. Poole, C. Carl, B. Sexton, F. Glenn, S. Whalan, R. De Nys, *Biofouling* **2014**, 30, 1; b) J. F. Schumacher, N. Aldred, M. E. Callow, J. A. Finlay, J. A. Callow, A. S. Clare, A. B. Brennan, *Biofouling* **2007**, 23, 307; c) A. V. Bers, M. Wahl, *Biofouling* **2004**, 20, 43; d) J. F. Schumacher, M. L. Carman, T. G. Estes, A. W. Feinberg, L. H. Wilson, M. E. Callow, J. A. Callow, J. A. Finlay, A. B. Brennan, *Biofouling* **2007**, 23, 55; e) M. L. Carman, T. G. Estes, A. W. Feinberg, J. F. Schumacher, W. Wilkerson, L. H. Wilson, M. E. Callow, J. A. Callow, A. B. Brennan, *Biofouling* **2006**, 22, 11.

[11] a) E. P. Ivanova, J. Hasan, H. K. Webb, G. Gervinskas, S. Juodkazis, V. K. Truong, A. H. F. Wu, R. N. Lamb, V. A. Baulin, G. S. Watson, J. A. Watson, D. E. Mainwaring, R. J. Crawford, *Nature Communications* **2013**, 4, 2838; b) D. P. Linklater, M. De Volder, V. A. Baulin, M. Werner, S. Jessl, M. Golozar, L. Maggini, S. Rubanov, E. Hanssen, S. Juodkazis, *ACS nano* **2018**, 12, 6657; c) S. Pogodin, J. Hasan, V. A. Baulin, H. K. Webb, V. K. Truong, T. H. P. Nguyen, V. Boshkovikj, C. J. Fluke, G. S. Watson, J. A. Watson, *Biophysical journal* **2013**, 104, 835; d) E. P. Ivanova, J. Hasan, H. K. Webb, V. K. Truong, G. S. Watson, J. A. Watson, V. A. Baulin, S. Pogodin, J. Y. Wang, M. J. Tobin, *Small* **2012**, 8, 2489; e) S.-H. Hong, J. Hwang, H. Lee, *Nanotechnology* **2009**, 20, 385303; f) S. Pandit, K. Gaska, V. R. Mokkapati, E. Celauro, A. Derouiche, S. Forsberg, M. Svensson, R. Kádár, I. Mijakovic, *Small* **2020**, 1904756; g) J. Jenkins, J. Mantell, C. Neal, A. Gholinia, P. Verkade, A. H. Nobbs, B. Su, *Nature Communications* **2020**, 11, 1626;

h) S. G. Higgins, M. Becce, A. Belessiotis‐Richards, H. Seong, J. E. Sero, M. M. Stevens, *Advanced Materials* **2020**, 1903862.

[12] a) M. Wahl, *Marine ecology progress series* **1989**, 58, 175; b) D. M. Yebra, S. Kiil, K. Dam-Johansen, *Progress in organic coatings* **2004**, 50, 75; c) L. D. Chambers, K. R. Stokes, F. C. Walsh, R. J. Wood, *Surface and Coatings Technology* **2006**, 201, 3642; d) C. M. Magin, S. P. Cooper, A. B. Brennan, *Materials today* **2010**, 13, 36.

[13] a) T. L. Liu, C.-J. C. Kim, *Science* **2014**, 346, 1096; b) H. J. Fan, P. Werner, M. Zacharias, *small* **2006**, 2, 700; c) C. Vieu, F. Carcenac, A. Pepin, Y. Chen, M. Mejias, A. Lebib, L. Manin-Ferlazzo, L. Couraud, H. Launois, *Applied surface science* **2000**, 164, 111.

[14] a) M. P. Stoykovich, M. Müller, S. O. Kim, H. H. Solak, E. W. Edwards, J. J. De Pablo, P. F. Nealey, *Science* **2005**, 308, 1442; b) O. Ikkala, G. ten Brinke, *science* **2002**, 295, 2407; c) S. Mann, *Nature materials* **2009**, 8, 781.

[15] a) A. R. Bielinski, M. Boban, Y. He, E. Kazyak, D. H. Lee, C. Wang, A. Tuteja, N. P. Dasgupta, *ACS nano* **2016**, 11, 478; b) A. R. Bielinski, E. Kazyak, C. M. Schlepütz, H. J. Jung, K. N. Wood, N. P. Dasgupta, *Chemistry of Materials* **2015**, 27, 4799.

[16] Y. Chen, N. J. Ginga, W. S. LePage, E. Kazyak, A. J. Gayle, J. Wang, R. E. Rodríguez, M. D. Thouless, N. P. Dasgupta, *ACS Applied Materials & Interfaces* **2019**, DOI: 10.1021/acsami.9b15193.

[17] R. N. Wenzel, *Industrial & Engineering Chemistry* **1936**, 28, 988.

[18] a) A. Lafuma, D. Quéré, *Nature materials* **2003**, 2, 457; b) A. Checco, B. M. Ocko, A. Rahman, C. T. Black, M. Tasinkevych, A. Giacomello, S. Dietrich, *Physical Review Letters* **2014**, 112, 216101.

[19] W. Choi, A. Tuteja, J. M. Mabry, R. E. Cohen, G. H. McKinley, *Journal of colloid and interface science* **2009**, 339, 208.

[20] J. Monty, E. Dogan, R. Hanson, A. Scardino, B. Ganapathisubramani, N. Hutchins, *Biofouling* **2016**, 32, 451.

[21] a) K. Z. Hunsucker, A. Koka, G. Lund, G. Swain, *Biofouling* **2014**, 30, 1133; b) S. V. Dobretsov, P.-Y. Qian, *Biofouling* **2002**, 18, 217.

[22] G. B. Hwang, K. Page, A. Patir, S. P. Nair, E. Allan, I. P. Parkin, *ACS Nano* **2018**, 12, 6050.

[23] a) T. Diu, N. Faruqui, T. Sjöström, B. Lamarre, H. F. Jenkinson, B. Su, M. G. Ryadnov, *Scientific reports* **2014**, 4, 7122; b) Y. Q. Li, B. Zhu, Y. Li, W. R. Leow, R. Goh, B. Ma, E. Fong, M. Tang, X. Chen, *Angewandte Chemie International Edition* **2014**, 53, 5837.

[24] Y. Song, U. Kadiyala, P. Weerappuli, J. J. Valdez, S. Yalavarthi, C. Louttit, J. S. Knight, J. J. Moon, D. S. Weiss, J. S. VanEpps, *Advanced Materials* **2019**, 31, 1807436.

[25] F. Wu, B. J. Harper, S. L. Harper, *Environmental Toxicology and Chemistry* **2019**, 38, 591.

[26] W. Hu, C. Peng, W. Luo, M. Lv, X. Li, D. Li, Q. Huang, C. Fan, *ACS nano* **2010**, 4, 4317.

[27] Y. Tu, M. Lv, P. Xiu, T. Huynh, M. Zhang, M. Castelli, Z. Liu, Q. Huang, C. Fan, H. Fang, *Nature nanotechnology* **2013**, 8, 594.

[28] a) K. Holmén, P. Liss, *Tellus B: Chemical and Physical Meteorology* **1984**, 36, 92; b) R. Poetes, K. Holtzmann, K. Franze, U. Steiner, *Physical review letters* **2010**, 105, 166104.

[29] P. R. Jones, X. Hao, E. R. Cruz-Chu, K. Rykaczewski, K. Nandy, T. M. Schutzius, K. K. Varanasi, C. M. Megaridis, J. H. Walther, P. Koumoutsakos, *Scientific reports* **2015**, 5, 12311.

[30] K. Golovin, M. Boban, J. M. Mabry, A. Tuteja, *ACS Applied Materials & Interfaces* **2017**, 9, 11212.

[31] a) L. Wang, T. J. McCarthy, *Angewandte Chemie International Edition* **2016**, 55, 244; b) J. Wang, L. Wang, N. Sun, R. Tierney, H. Li, M. Corsetti, L. Williams, P. K. Wong, T.-S. Wong, *Nature Sustainability* **2019**, 2, 1097; c) L. Zhang, Z. Guo, J. Sarma, X. Dai, *ACS Applied Materials & Interfaces* **2020**, 12, 20084.